Enhanced charge ordering transition in doped $CaFeO_3$ through steric templating

Lai Jiang,[1] Diomedes Saldana-Greco,[1] Joseph T. Schick,[2] and Andrew M. Rappe[1,*]

[1]*The Makineni Theoretical Laboratories, Department of Chemistry, University of Pennsylvania, Philadelphia, Pennsylvania 19104, USA*

[2]*Department of Physics, Villanova University, Villanova, Pennsylvania 19085, USA*

(Received 24 February 2014; published 5 June 2014)

We report a density functional theory investigation of B-site doped $CaFeO_3$, a prototypical charge ordered perovskite. At 290 K, $CaFeO_3$ undergoes a metal-insulator transition and a charge disproportionation reaction $2Fe^{4+} \rightarrow Fe^{5+} + Fe^{3+}$. We observe that when Zr dopants occupy a (001) layer, the band gap of the resulting solid solution increases to 0.93 eV due to a two-dimensional Jahn-Teller-type distortion, where FeO_6 cages on the xy plane elongate along x and y alternatively between neighboring Fe sites. Furthermore, we show that the rock-salt ordering of the Fe^{5+} and Fe^{3+} cations can be enhanced when the B-site dopants are arranged in a (111) plane due to a collective steric effect that facilitates the size discrepancy between the $Fe^{5+}O_6$ and $Fe^{3+}O_6$ octahedra and therefore gives rise to a larger band gap. The enhanced charge disproportionation in these solid solutions is verified by rigorously calculating the oxidation states of the Fe cations with different octahedral cage sizes. We therefore predict that the corresponding transition temperature will increase due to the enhanced charge ordering and larger band gap. The compositional, structural, and electrical relationships exploited in this paper can be extended to a variety of perovskites and nonperovskite oxides, providing guidance in the structural manipulation of electrical properties of functional materials.

DOI: 10.1103/PhysRevB.89.235106 PACS number(s): 71.30.+h, 75.25.Dk, 81.30.Hd

I. INTRODUCTION

The perovskite (ABO_3) family of materials has been paid considerable attention, both in experimental and theoretical studies, due to its flexible and coupled compositional, structural, electrical, and magnetic properties [1–3]. Such flexibility arises from the structural building blocks—the corner-connected BO_6 octahedra, where B is usually a transition metal. Typical structural variations from the cubic structure include rotation and tilting of the octahedra [4], off-centering of the A and/or B cations (pseudo-Jahn-Teller effect) [5], and expansion/contraction of the BO_6 octahedral cages [6]. While the first two distortions are ubiquitous, the cooperative octahedral breathing distortion is rather rare in perovskites with a single B-cation composition. Such breathing distortion, resulting from the alternation of elongation and contraction of the B-O bonds between neighboring BO_6 cages, is usually concomitant with the charge ordering of the B cations and a corresponding metal-insulator transition. $CaFeO_3$ is a typical perovskite material exhibiting such charge ordering transition [7]. At room temperature, the strong covalency in the Fe e_g–O $2p$ interaction leads to a σ^* band and electron delocalization, which gives rise to metallic conductivity in $CaFeO_3$. Near 290 K, a second-order metal-insulator transition (MIT) occurs, which reduces the conductivity dramatically [8]. The Mössbauer spectrum of low-temperature $CaFeO_3$ has revealed the presence of two chemically distinct Fe sites (with different hyperfine fields) that are present in equal proportion [9]. This indicates that the Fe cations undergo charge disproportionation $2Fe^{4+} \rightarrow Fe^{5+} + Fe^{3+}$ below the transition temperature. The origin of the charge ordering transition is usually attributed to Mott insulator physics, where the carriers are localized by strong electron-lattice interactions [7,9–11]. More recently, it has been debated whether the difference in charge state resides on the B cations or as holes in the oxygen $2p$ orbitals [12–14], and several computational studies showed that the magnetic configuration, in addition to structural changes, plays a vital role in stabilizing the charge ordered state in $CaFeO_3$ [15–17]. Nevertheless, the amplitude of the cooperative breathing mode is a key indicator of the magnitude of electron trapping and band-gap opening in MIT. Conversely, because the MIT is sensitive to lattice distortion, structural manipulation such as cation doping and epitaxial strain can be exploited to control the electrical properties of this family of oxide systems.

In this study, we examine the structural and electrical properties in B-cation doped $CaFeO_3$ with density functional theory (DFT). Various dopant cations, concentrations, and arrangements have been tested. Dopants of different sizes are tested, and alignments of pairs of dopants along different crystallographic planes are examined. To confirm the presence of charge ordering in (111) doped $CaFeO_3$, we also carried out rigorous oxidation state calculations for Fe cations in different octahedral cages based on their wave-function topologies [18]. Through examination of these model systems, we assess the extent to which the structure-coupled electronic transition in doped oxide materials such as $CaFeO_3$ can be influenced via doping to enhance band-gap tunability, which in turn controls the MIT temperature.

II. METHODOLOGY

Our DFT calculations are performed using the norm-conserving nonlocal pseudopotential plane-wave method [19]. The pseudopotentials [20] are generated by the OPIUM package [21] with a 50 Ry plane-wave energy cutoff. Calculations are performed with the QUANTUM-ESPRESSO package [22] using the local-density approximation [23] with the rotationally invariant effective Hubbard U correction [24] of 4 eV on the Fe d orbitals [17,25] for the exchange-correlation functional. In the case of Ni and Ce doping, we applied $U = 4.6$ eV [26] and $U = 5$ eV [27] for Ni d and Ce

*rappe@sas.upenn.edu

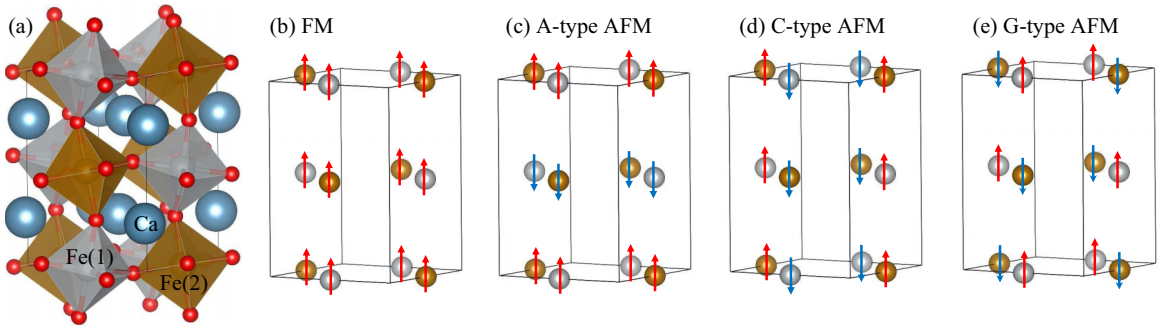

FIG. 1. (Color online) (a) Low-temperature $P2_1/n$ structure of $CaFeO_3$ with two symmetry-distinct Fe cation sites color coded. The spin ordering of the Fe cations are (b) ferromagnetic (FM), (c) A-type antiferromagnetic (AFM), (d) C-type antiferromagnetic, and (e) G-type antiferromagnetic.

f, respectively. Calculations are performed on a $4 \times 4 \times 4$ Monkhorst-Pack k-point grid [28] with electronic energy convergence of 1×10^{-8} Ry, force convergence threshold of 2×10^{-4} Ry/Å, and pressure convergence threshold of 0.5 kbar. For polarization calculations, a $4 \times 6 \times 12$ k-point grid is used, where the densely sampled direction is permuted in order to obtain all three polarization components. Different spin orderings for pure $CaFeO_3$ are tested to find the magnetic ground state, and subsequent solid solution calculations all start with that magnetic ground state.

III. RESULTS AND DISCUSSION

A. Ground state of $CaFeO_3$ and $CaZrO_3$

To identify the correct spin ordering in pure $CaFeO_3$, we performed relaxations on both high-temperature metallic orthorhombic $Pbnm$ [7,9,11,29] and low-temperature semiconducting monoclinic $P2_1/n$ [30] structures with common magnetic orderings commensurate with the $2 \times 2 \times 2$ supercells, as shown in Fig. 1 [note that diamagnetic (DM) ordering is not included in the figure].

From the results in Table I, we can see that both high-temperature and low-temperature ferromagnetic $CaFeO_3$ relax to the ferromagnetic ground states. Note that an additional magnetic phase transition is experimentally observed for $CaFeO_3$ at 15 K, where it adopts an incommensurate magnetic structure with a modulation vector $[\delta, 0, \delta]$ ($\delta \approx 0.32$, and reciprocal lattice vectors as basis) [7]. Since DFT calculates 0 K internal energy, the ferromagnetic ground state represents a reasonable approximation of the spin-spin interactions within a unit cell given the relatively long spin-wave length and low experimental crossover temperature to FM. The volumes of the two FeO_6 cages are equivalent in the high-temperature metallic phase, as expected. The low-temperature ground state has a cage size difference, $\Delta V = 0.41$Å^3, indicating some degree of charge ordering. However, the projected density of states (PDOS) of the $P2_1/n$ ground-state $CaFeO_3$ in Fig. 2(a) shows that although there are separate gaps in each spin channel, the valence-band edge in the majority spin touches the conduction-band edge in the minority spin, resulting in zero total gap. The absence of band gap and the weak charge ordering is a result of the underestimation of band gaps in DFT [31] due to its unphysical electron delocalization. This result is common in Mott insulators with partially filled d orbitals and is in agreement with another DFT study of $CaFeO_3$ [12]. Even though DFT does not predict the correct electronic ground state of $CaFeO_3$, it is, however, indicative of the sensitive nature of the $CaFeO_3$ band gap as it can be easily influenced when Fe d orbital filling is varied by structural or other perturbations. Moreover, the different ΔV between high temperature and low temperature of the FeO_6 ground state suggests that the structural aspect of the MIT can be modeled reasonably well by DFT.

TABLE I. Calculated total energy E, atomic magnetization m_1 and m_2 for the two Fe sites, total magnetization per five-atom formula unit M, and FeO_6 octahedral volume V_1 and V_2 for the two Fe sites of relaxed $CaFeO_3$ with different starting structures and magnetic orderings.

	E (eV)	m_1 (μ_B)	m_2 (μ_B)	M (μ_B)	V_1 (Å^3)	V_2 (Å^3)
$Pbnm$						
DM	6.64	N/A	N/A	N/A	8.40	8.40
FM	0.07	3.38	3.38	4.00	8.94	8.94
A-AFM	0.43	3.29	−3.29	0.00	9.00	9.00
C-AFM	0.58	3.24	−3.24	0.00	8.92	8.92
G-AFM	0.96	3.44	−3.51	0.06	9.52	8.47
$P2_1/n$						
DM	6.64	N/A	N/A	N/A	8.40	8.40
FM	0	3.13	3.60	4.00	9.16	8.75
A-AFM	0.32	3.69	−3.69	0.00	9.57	8.40
C-AFM	0.58	3.24	−3.24	0.00	8.92	8.92
G-AFM	0.81	3.85	−2.39	1.00	10.05	8.13

For comparison, we calculated the PDOS of $CaZrO_3$ relaxed from the experimental $Pbmn$ structure [32], also shown in Fig. 2(b). Because Zr^{4+} has empty $4d$ orbitals, the fraction of Zr d states in the valence band is negligible compared to O p states, and a wide charge-transfer gap of 3.82 eV occurs. Since we expect to exploit the size effect of the dopants such as Zr to influence the electronic property of $CaFeO_3$, we expect that the nature of the Fe spin-spin interaction is not greatly affected by doping. Therefore, in the following study, we continue to use FM as the starting magnetic configuration for relaxations of the doped materials.

B. $CaFeO_3$-$CaZrO_3$ solid solutions with $2 \times 2 \times 2$ super cell

To test how Zr doping influences the structural and electrical properties of $CaFeO_3$, we performed relaxations and

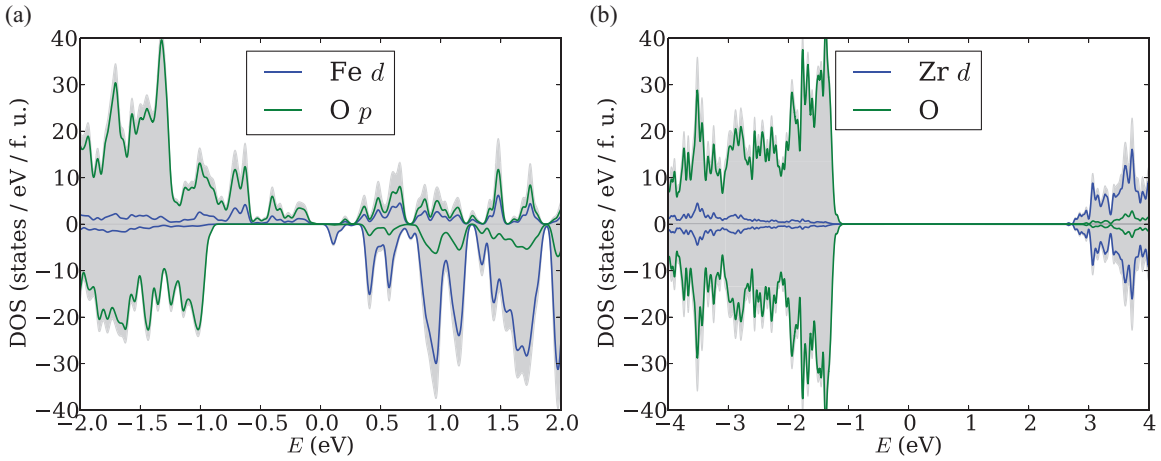

FIG. 2. (Color online) Projected density of states of (a) $CaFeO_3$ (left) and (b) $CaZrO_3$.

subsequent band-gap calculations of $CaFeO_3$-$CaZrO_3$ solid solutions. We employ a $2 \times 2 \times 2$ super cell and explore all possible B-site cation combinations. All of the solid solutions tested turn out to be metallic except one, which has a gap of 0.93 eV. The insulating solid solution has a cation arrangement with four Zr cations on the (001) plane, making it a layered structure along [001]. Interestingly, instead of a breathing-mode charge disproportionation, this structure has a two-dimensional (2D) Jahn-Teller-type distortion, and all four Fe cations are in the same chemical environment. As shown in Fig. 3, the Fe-O bond lengths in the xy plane are 2.16 Å and 1.83 Å in each FeO_6, with the orientation alternating between neighbors. The shorter Fe-O bond length is essentially the same as that in high-temperature $CaFeO_3$. The consequence of the addition of larger Zr^{4+} cations ($r = 0.72$ Å) compared to Fe^{4+} ($r = 0.59$ Å) is that when Zr cations occupy an entire (001) plane, the in-plane lattice is expanded from 3.70 Å to 3.88 Å, elongating the Fe-O bonds and enabling the 2D Jahn-Teller-type distortion.

From the PDOS of the solid solution in Fig. 4(a), we can see that like pure $CaFeO_3$, both the valence and the conduction edges are of Fe $3d$ and O $2p$ characters, with virtually no Zr contribution. In charge ordering MIT, the delocalized electrons on Fe^{4+} transfer to neighboring Fe^{4+}, making Fe^{3+}/Fe^{5+} pairs with the valence and conduction bands located on different cations, concomitant with FeO_6 cage size changes. The band gap in the case of charge ordering therefore depends on the energy difference between the e_g orbitals in Fe^{3+} and Fe^{5+}, which in turn is affected by the crystal-field splitting energy caused by the oxygen ligands. On the other hand, as illustrated in Fig. 4(b), the solid solution band gap is caused by the removal of degeneracy in the e_g orbitals and is controlled by the difference in energy between the two e_g orbitals on the same Fe^{4+} cation. Since the e_g gap splitting is a result of the Fe-O bond length difference, it is easier to tune by applying either chemical pressure or biaxial strain to change the in-plane lattice constant, whereas the charge ordering mechanism requires the control of individual FeO_6 octahedral sizes to change the relative energy of e_g orbitals between two Fe sites. Nevertheless, this $CaFeO_3$-$CaZrO_3$ solid solution demonstrates that when arranged in a particular way, in this case on the (001) plane, the size effect of the large Zr cation can cause a cooperative steric effect on the structure and affect the electrical properties of $CaFeO_3$, opening up the band gap via a completely different mechanism.

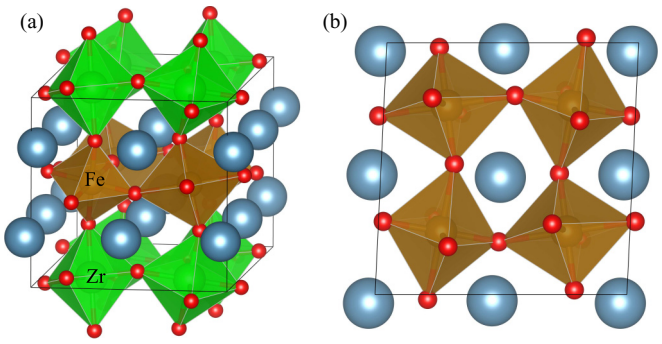

FIG. 3. (Color online) (a) Crystal structure of $Ca(Fe_{1/2}Zr_{1/2})O_3$ and (b) top view of the ZrO_2 layer showing the 2D Jahn-Teller-type distortion.

C. $CaFeO_3$ with dopants on the (111) plane

As discussed in the previous section, simply doping Zr into $2 \times 2 \times 2$ $CaFeO_3$ does not increase the band gap, except for one case where 2D Jahn-Teller instead of breathing mode serves to make the system insulating. In a perovskite system with rock-salt ordered alternating B cations, such as $CaFeO_3$, one B-cation type occupies entire (111) planes and the other type occupies its neighbors in all directions. Since Zr cation is larger than Fe cation, to fully utilize its steric effect to distinguish Fe^{3+} from Fe^{5+}, it follows that Zr should replace a full Fe^{3+} plane to increase the BO_6 size on the plane, maximizing its utility by enhancing the cage size difference. A schematic of the (111) doping strategy and the influence of the dopants on their neighboring planes is shown in Fig. 5(b).

Following this logic, we perform calculations with a $\sqrt{2} \times \sqrt{6} \times 2\sqrt{3}$ $CaFeO_3$ super cell, which has six (111) FeO_2 layers stacked perpendicularly, as the parent material. One layer of Fe atoms is replaced with Zr atoms and the structure is then relaxed. The final structure is shown in Fig. 5(a), as well as the average BO_6 cage size of each layer. Clearly, the introduction

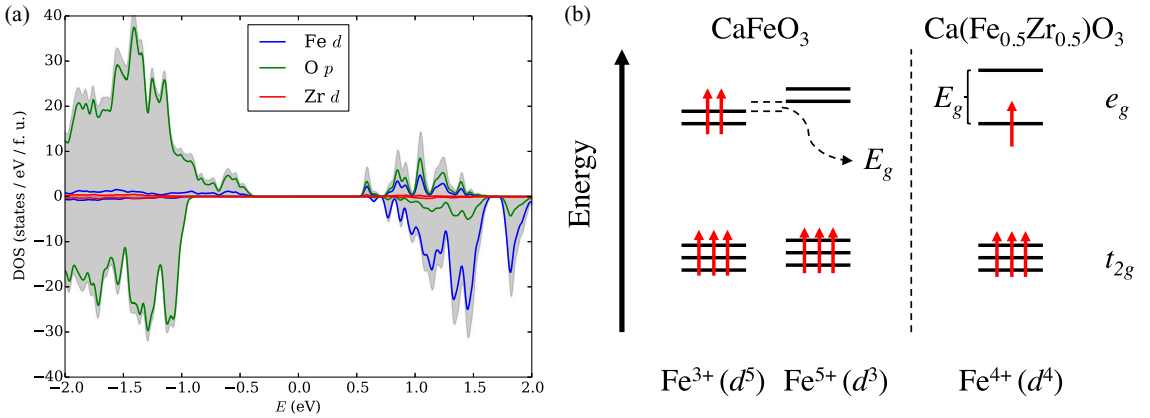

FIG. 4. (Color online) (a) PDOS of $Ca(Fe_{1/2}Zr_{1/2})O_3$ and (b) illustration of band-gap formation in $CaFeO_3$ (left) and $Ca(Fe_{1/2}Zr_{1/2})O_3$ (right).

of a (111) Zr layer drives the charge disproportionation of Fe^{4+} by exerting chemical pressure on both sides of the layer and favoring the FeO_6 on the two adjacent planes to be smaller and become Fe^{5+}. The second-next-neighboring layers in turn have more room to expand and favor larger Fe^{3+}. The size difference between the largest and the smallest FeO_6 cages ($\Delta V = 0.58$ Å^3) in this structure is an enhancement compared to pure $CaFeO_3$ $\Delta(V = 0.41$ Å^3), which suggests the presence of a stronger charge ordering and a wider band gap. However, electronic structure calculation shows that this solid material is metallic as well. The reason that the seemingly more charge ordered system still does not possess a gap can be attributed to the supercell employed. By using a unit cell with six (111) layers and replacing only one layer of Fe with Zr, the remaining five Fe layers are structurally disturbed by the large Zr layer, as expected. However, the charge disproportionation reaction $2Fe^{4+} \rightarrow Fe^{5+} + Fe^{3+}$ cannot proceed to completion because it requires an even number of Fe layers. Therefore, with one layer of dopants, there will always be Fe^{4+} "leftovers" that render the whole system metallic.

To resolve the issue of odd number of Fe layers, we introduce another layer of +4 dopants with smaller ionic radius than Fe. For simplicity, we denote a solid solution in this case by listing the B cations in each of its six (111) layers, with dopant elements in bold. For example, the previously discussed one-layer Zr-doped solid solution would be denoted as **Zr**FeFeFeFeFe. The presence of two dopant layers provides both positive and negative chemical pressure to expand Fe^{3+} and contract Fe^{5+}. These two dopant layers are separated by an even number of Fe layers so that the FeO_6 size alternation is enhanced. An odd number of Fe layers in between the dopant layers would disrupt and impede the size modulation period. Relaxations are performed on **ZrNi**FeFeFeFe and **Zr**FeFe**Ni**FeFe, as well as **CeNi**FeFeFeFe and **Ce**FeFe**Ni**FeFe. The average FeO_6 cage size per layer is listed in Table II, along with the maximum cage size difference ΔV and the corresponding band gap of each solid solution. It can be seen that with only Zr as dopant, the ΔV is significantly smaller than those with two layers of dopants, and ΔV correlates with the band gap. The Ce-containing solid solutions have a larger ΔV compared to the Zr-containing

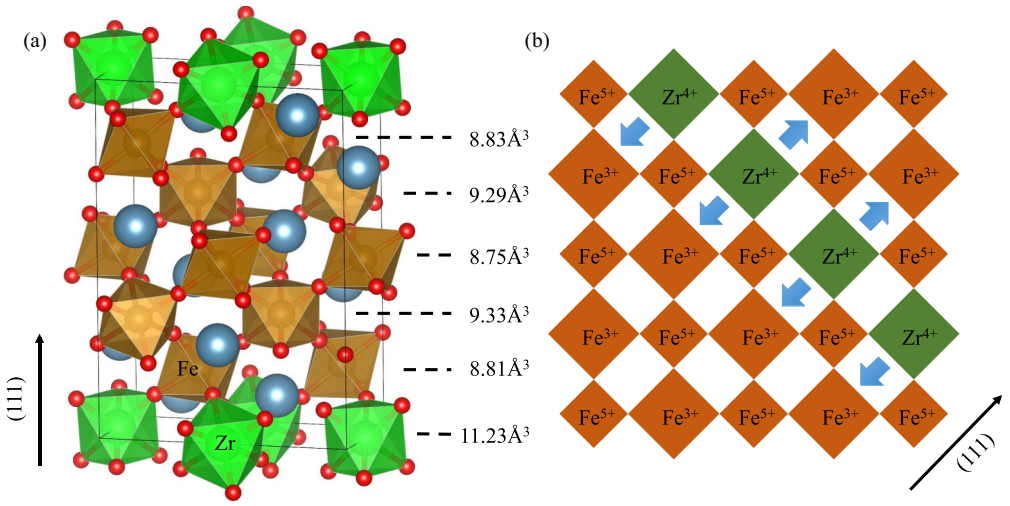

FIG. 5. (Color online) (a) Crystal structure of a $\sqrt{2} \times \sqrt{6} \times 2\sqrt{3}$ $CaFeO_3$ supercell doped with one layer of Zr on the (111) plane. The average BO_6 octahedron size is listed on the side. (b) Schematic of how a layer of dopants with larger ionic radius exerts a cooperative size effect on the neighboring layers and enhances the existing charge ordering.

TABLE II. Properties of $CaFeO_3$ doped on the (111) plane. V_1 through V_6 are average FeO_6 volumes in Å^3, where the largest and the smallest cages in each solid solution are in bold. ΔV is the size difference between the largest and smallest volumes and E_g is the band gap of the corresponding material in eV.

(111) layers	V_1	V_2	V_3	V_4	V_5	V_6	ΔV	E_g
ZrFeFeFeFeFe	Zr	8.81	**9.33**	**8.75**	9.29	8.83	0.58	0
ZrNiFeFeFeFe	Zr	Ni	9.52	8.53	**9.59**	**8.27**	1.32	0.49
ZrFeFe**Ni**FeFe	Zr	8.32	9.43	Ni	**9.45**	**8.28**	1.17	0.11
CeNiFeFeFeFe	Ce	Ni	**9.77**	8.61	9.69	**8.29**	1.48	0.83
CeFeFe**Ni**FeFe	Ce	**8.39**	**9.75**	Ni	9.73	8.41	1.36	0.53

ones, due to the larger size of Ce. It also shows that when the larger dopant and the smaller dopant layers are adjacent, the resulting ΔV is larger than when they are two Fe layers apart; this is due to the lack of symmetry of the former configuration where the absence of a mirror plane perpendicular to the z axis allows for the FeO_6 close to the dopant layers to further expand or contract compared to the ones that are not neighbors of the dopant layers. In the latter configuration, symmetry guarantees that octahedra on either side of the dopant layer are deformed equally.

From Fig. 6, we can see that with increasing difference in FeO_6 size, the band gap of the corresponding solid solutions increases accordingly. This relationship demonstrates the coupling between structural and electrical properties as larger FeO_6 size discrepancy indicates stronger and more complete charge disproportionation. As illustrated in Fig. 4(b), when charge ordering is the band-gap opening mechanism, the gap size depends on the crystal-field splitting energy difference between Fe^{3+} and Fe^{5+}. A larger FeO_6 cage size difference means that the O $2p$–Fe $3d$ repulsion difference is also larger between the two Fe sites. This causes the energy difference of the e_g orbitals in the two sites to increase and the band gap to increase as well. Using linear regression, we estimate that the chemical pressure exerted on the band gap by the volume difference in this type of solid solution is quite large, at about 370 GPa, in accordance with the effective band-gap tuning. Since the transition to metal occurs when thermally activated electrons have enough energy to cross the band gap and flow between the two Fe sites to make them indistinguishable, we believe that by (111) doping, the MIT temperature of $CaFeO_3$ can be increased, making devices based on it more operable at room temperature.

To investigate the layered nature of the solid solutions, we use **ZrNi**FeFeFeFe as an example and plot the projected density of states of it in Fig. 7 in a layer-resolved fashion. Each of the six panels in Fig. 7 represents a layer of $CaBO_3$, and the relative position of the panels corresponds to that of the six layers in the crystal. It can be seen clearly that for the four layers containing Fe ions, the first and the third layers have more majority-spin Fe d in the valence band, while the second and fourth layers have more majority-spin Fe d in the conduction band. This difference is consistent with the fact that Fe^{3+} has more filled d orbitals than Fe^{5+}, and supports our prediction that the doubly doped (111) layered $CaFeO_3$ has an enhanced charge ordering due to the strong modulation of the FeO_6 cage volume.

To further verify the charge disproportionation mechanism, we performed oxidation state calculations of the Fe cations in **ZrNi**FeFeFeFe. We employed an unambiguous oxidation state definition [18] based on wave-function topology, whereby moving a target ion to its image site in an adjacent cell through

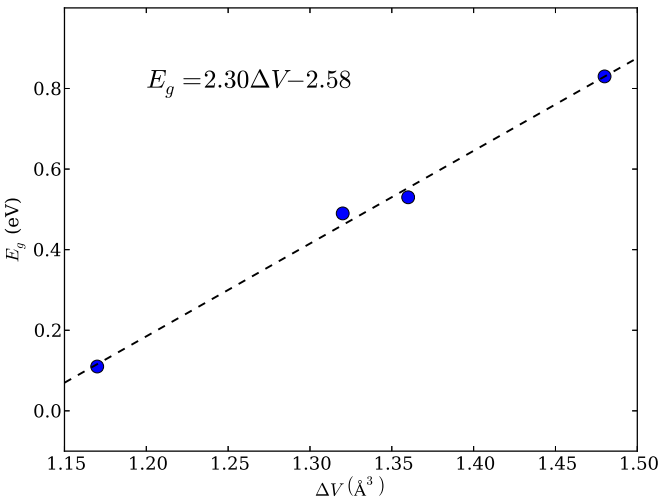

FIG. 6. (Color online) Band gap E_g of the (111) doped $CaFeO_3$ solid solutions increases with the corresponding maximum FeO_6 size difference ΔV. This gives an effective chemical pressure on the band gap of 2.30 eV/Å^3 or 370 GPa.

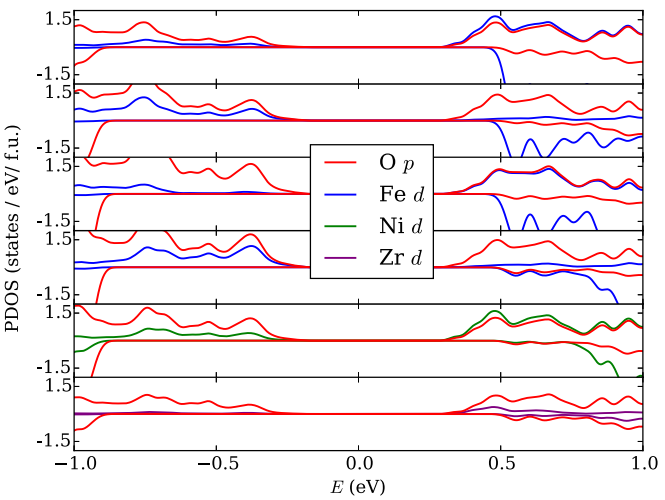

FIG. 7. (Color online) Layer-resolved projected density of states of **ZrNi**FeFeFeFe. Each of the six panels represents a layer of $CaBO_3$, and the relative position of the panels corresponds to that of the six layers in the crystal.

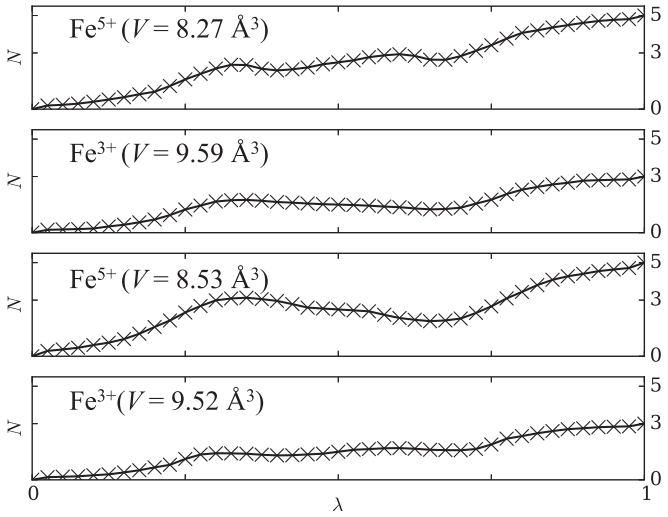

FIG. 8. Oxidation state N of the four Fe cations. λ denotes the reaction coordinate of moving the Fe ion sublattice to the neighboring cell, and the change in $N = \Delta \frac{\vec{P}\cdot\vec{R}}{\vec{R}^2}$ from $\lambda = 0$ to $\lambda = 1$ corresponds to the oxidation state of that Fe ion.

an insulating path and calculating the polarization change during the process, the number of electrons that accompany the moving nucleus can be calculated. The oxidation state obtained this way is guaranteed to be an integer and is unique for an atom in a given chemical environment, not dependent on other factors such as charge partitioning or the choice of orbital basis. In Fig. 8, we show how the quantity $N = \Delta\vec{P}\cdot\vec{R}/\vec{R}^2$ changes as each Fe cation is moved along an insulating path to the next cell, which is equivalent to the oxidation state of the cation. The two Fe ions with larger cages are confirmed to be Fe^{3+} and the ones with smaller cages are Fe^{5+}. This proves that charge ordering occurs in this material and causes band-gap opening. Note that the oxidation states calculated are not directly related to the charges localized around the Fe sites, which has been shown to change insignificantly upon oxidation reaction in some cases [33]. In fact, the Bader charge [34] of the Fe cations is 1.76 and 1.73 for the smaller and larger FeO_6 cages, respectively, which shows minuscule differences between Fe sites that are in significantly different chemical environments in terms of oxygen ligand attraction.

The (111) doping strategy shows that the size difference between Fe^{3+} and Fe^{5+} can be exploited and reinforced by selectively replacing layers of Fe^{3+} with Fe^{5+} with atoms of even larger or smaller size, respectively, to enhance charge ordering and the insulating character of the $CaFeO_3$ system.

IV. CONCLUSIONS

We have demonstrated that for prototypical charge ordering perovskite $CaFeO_3$, the band gap of the insulating state can be engineered by B-site cation doping and structural manipulation. For the dopant atoms to exert significant influence on the parent material, it is favorable to arrange them in a way that their size effects are cooperative and synergistic, producing a collective steric effect and greatly altering the structural and electrical properties. When doped on the (001) plane with larger Zr cations, the in-plane lattice constant expands and supports a 2D Jahn-Teller-type distortion, where each FeO_6 has two distinct Fe-O bond lengths in the xy plane. Such distortion removes the degeneracy of the two e_g orbitals on each Fe^{4+} and opens up a band gap (not caused by charge ordering) of 0.93 eV. On the other hand, to enhance the weak charge ordering in pure $CaFeO_3$, we discovered that including two types of dopants on the (111) plane can increase the FeO_6 cage size difference and enhance the charge ordering. Using Zr or Ce to replace the larger Fe^{3+} and Ni to replace the smaller Fe^{5+} increases the band gap up to 0.83 eV. The degree of charge ordering is closely related to the magnitude of FeO_6 cage size difference. We used the rigorous definition of oxidation state to verify that in the latter case, the band-gap opening mechanism is indeed charge disproportionation, as the oxidation states of the larger and smaller Fe cations are calculated to be +3 and +5, respectively. Our results show that the structural and electrical properties of $CaFeO_3$ are coupled, and simple steric effects can enhance charge ordering transition and alter the band gap of the material greatly when the dopant atoms are placed to act cooperatively. Lastly, by enhancing the charge ordering via doping, we predict that the MIT temperature of $CaFeO_3$ can also be increased to a temperature more suitable for practical device operation.

ACKNOWLEDGMENTS

L.J. was supported by the Air Force Office of Scientific Research under Grant No. FA9550-10-1-0248. D.S.G. was supported by the US Department of Energy Office of Basic Energy Sciences under Grant No. DE-FG02-07ER15920. J.T.S. was supported by a sabbatical granted by Villanova University. A.M.R. was supported by the US Office of Naval Research under Grant No. N00014-11-1-0664. Computational support was provided by the High Performance Computing Modernization Office of the US Department of Defense, and the National Energy Research Scientific Computing Center of the US Department of Energy.

[1] L. Bellaiche, A. Garcia, and D. Vanderbilt, Phys. Rev. Lett. **84**, 5427 (2000).
[2] Y. Saito, H. Takao, T. Tani, T. Nonoyama, K. Takatori, T. Homma, T. Nagaya, and M. Nakamura, Nature (London) **432**, 84 (2004).
[3] D. I. Bilc and D. J. Singh, Phys. Rev. Lett. **96**, 147602 (2006).
[4] A. M. Glazer, Acta Cryst. **28**, 3384 (1972).
[5] T. Qi, I. Grinberg, and A. M. Rappe, Phys. Rev. B **82**, 134113 (2010).
[6] T. Thonhauser and K. M. Rabe, Phys. Rev. B **73**, 212106 (2006).
[7] P. M. Woodward, D. E. Cox, E. Moshopoulou, A. W. Sleight, and S. Morimoto, Phys. Rev. B **62**, 844 (2000).
[8] S. Kawasaki, M. Takano, R. Kanno, T. Takeda, and A. Fujimori, J. Phys. Soc. Jpn. **67**, 1529 (1998).
[9] M. Takano, N. Nakanishi, Y. Takeda, S. Naka, and T. Takada, Mater. Res. Bull. **12**, 923 (1977).
[10] A. J. Millis, Nature (London) **392**, 147 (1998).
[11] S. Ghosh, N. Kamaraju, M. Seto, A. Fujimori, Y. Takeda, S. Ishiwata, S. Kawasaki, M. Azuma, M. Takano, and A. K. Sood, Phys. Rev. B **71**, 245110 (2005).

[12] J. B. Yang, M. S. Kim, Q. Cai, X. D. Zhou, H. U. Anderson, W. J. James, and W. B. Yelon, J. Appl. Phys. **97**, 10A312 (2005).
[13] T. Akao, Y. Azuma, M. Usuda, Y. Nishihata, J. Mizuki, N. Hamada, N. Hayashi, T. Terashima, and M. Takano, Phys. Rev. Lett. **91**, 156405 (2003).
[14] T. Mizokawa, D. I. Khomskii, and G. A. Sawatzky, Phys. Rev. B **61**, 11263 (2000).
[15] T. Mizokawa and A. Fujimori, Phys. Rev. Lett. **80**, 1320 (1998).
[16] J. Ma, J.-Q. Yan, S. O. Diallo, R. Stevens, A. Llobet, F. Trouw, D. L. Abernathy, M. B. Stone, and R. J. McQueeney, Phys. Rev. B **84**, 224115 (2011).
[17] A. Cammarata and J. M. Rondinelli, Phys. Rev. B **86**, 195144 (2012).
[18] L. Jiang, S. V. Levchenko, and A. M. Rappe, Phys. Rev. Lett. **108**, 166403 (2012).
[19] M. C. Payne, M. P. Teter, D. C. Allan, T. A. Arias, and J. D. Joannopoulos, Rev. Mod. Phys. **64**, 1045 (1992).
[20] A. M. Rappe, K. M. Rabe, E. Kaxiras, and J. D. Joannopoulos, Phys. Rev. B **41**, 1227 (1990).
[21] http://opium.sourceforge.net
[22] P. Giannozzi, S. Baroni, N. Bonini, M. Calandra, R. Car, C. Cavazzoni, D. Ceresoli, G. L. Chiarotti, M. Cococcioni, I. Dabo, A. D. Corso, S. de Gironcoli, S. Fabris, G. Fratesi, R. Gebauer, U. Gerstmann, C. Gougoussis, A. Kokalj, M. Lazzeri, L. Martin-Samos, N. Marzari, F. Mauri, R. Mazzarello, S. Paolini, A. Pasquarello, L. Paulatto, C. Sbraccia, S. Scandolo, G. Sclauzero, A. P. Seitsonen, A. Smogunov, P. Umari, and R. M. Wentzcovitch, J. Phys.: Condens. Matter **21**, 395502 (2009).
[23] J. P. Perdew and A. Zunger, Phys. Rev. B **23**, 5048 (1981).
[24] K. A. Johnson and N. W. Ashcroft, Phys. Rev. B **58**, 15548 (1998).
[25] Z. Fang, K. Terakura, and J. Kanamori, Phys. Rev. B **63**, 180407 (2001).
[26] M. Cococcioni and S. de Gironcoli, Phys. Rev. B **71**, 035105 (2005).
[27] C. Loschen, J. Carrasco, K. M. Neyman, and F. Illas, Phys. Rev. B **75**, 035115 (2007).
[28] H. J. Monkhorst and J. D. Pack, Phys. Rev. B **13**, 5188 (1976).
[29] F. Kanamaru, H. Miyamoto, Y. Mimura, M. Koizumi, M. Shimada, S. Kume, and S. Shin, Mater. Res. Bull. **5**, 257 (1970).
[30] T. Saha-Dasgupta, Z. S. Popović, and S. Satpathy, Phys. Rev. B **72**, 045143 (2005).
[31] W. Kohn and L. J. Sham, Phys. Rev. **140**, A1133 (1965).
[32] I. Levin, T. G. Amos, S. M. Bell, L. Farber, T. A. Vanderah, R. S. Roth, and B. H. Toby, J. Solid State Chem. **175**, 170 (2003).
[33] P. H.-L. Sit, F. Zipoli, J. Chen, R. Car, M. H. Cohen, and A. Selloni, Chem. Eur. J. **17**, 12136 (2011).
[34] R. F. Bader, *A Quantum Theory* (Oxford University Press, Oxford, UK, 1990).